Augmenting a Nominal Assembly Motion Plan with a Compliant Behavior [1]

Gordon A. Dakin **Robin J. Popplestone**

Laboratory for Perceptual Robotics
University of Massachusetts
Amherst, MA 01003
dakin@cs.umass.edu, pop@cs.umass.edu

Abstract

A methodology is presented whereby a nominal trajectory for an assembly operation, computed from kinematic constraints alone, is augmented with a fine-motion strategy synthesized through uncertainty and force analyses. Insertion clearances and size tolerances are introduced into the assembly part models in parallel with the manual selection of a *perturbed nominal trajectory* in contact space. The selection of small clearances, and in turn, small insertion angles allows us to linearize contact space about discrete points in the nominal trajectory. Contact states are represented as affine spaces in a generalized C-space of model error and pose variables. The feasibility of proposed command velocities to be executed in the presence of position, control, and model error is determined through an uncertainty analysis technique based on the forward-projection of convex polytopes in contact space. Our approach further the automates the so-called "manual" methods of motion planning with uncertainty.

1 Introduction

In the *2-phase approach* to assembly motion planning, a nominal plan is first selected or derived with limited regard to the effects of sensor and control error, and then provisions are made to account for uncertainty. These provisions might entail refining the nominal plan (Taylor 1976) or augmenting the plan with constraints upon the initial conditions (Brooks 1982) or applied forces (Whitney 1982). The 2-phase approach differs from the *LMT* methods (Latombe 1989; Lozano-Pérez, Mason & Taylor 1984), in which the command motions themselves are derived to accommodate uncertainty. A drawback of the LMT approach is its time complexity of $O(2^{2^n})$ in the number of plan steps. An advantage of the 2-phase approach is that goal configurations and nominal trajectories may be derived in phase 1 from geometric constraints alone (Liu 1990; Popplestone, Ambler & Bellos 1980).

The approaches to motion planning with uncertainty that have been referred to by (Latombe 1989) as the "manual methods" were first developed for deriving applied force constraints to prevent jamming and wedging in the context of the *peg-in-hole problem* (Whitney 1982). (Caine 1985) developed designer tools for manually selecting a trajectory of assembly configurations, and for deriving applied wrench constraints to prevent jamming and the breaking of contact while traversing the specified contact states.

This paper focuses on the second phase of the 2-phase approach. Like the "designer" approach of Caine [3], our methodology does not exclude human participation in the development of a fine-motion strategy. Tools for generating and verifying a fine-motion plan permit one to juggle design variables including trajectory perturbations, clearances, and tolerances.

Input consists of a nominal mating trajectory derived by the high-level assembly motion planner KA3 (Liu 1990) from the feature symmetries of geometric models that permit zero clearance at the insertion sites. Small clearances and tolerances are added to these models, giving rise to local C-spaces of perturbations from discrete points in the nominal trajectory. The small insertion angles permitted by the narrow clearances warrant the linearization of these C-spaces, whose boundaries are characterized as sets of *linearized C-surfaces* in a generalized C-space of model error and pose variables. Linear programming-based tools are employed to confirm the existence and adjacency of polytopic contact states in the contact state lattice. Candidate command velocities to be executed in the presence of position, control, and model error are also verified via linear programming. The resulting fine motion strategy consists of an initial target pose and a sequence of command velocities in specified contact states. The generation of applied force constraints for maintaining jam–free contact in the specified states is described elsewhere (Dakin 1991).

[1] Preparation of this paper was supported by grant number N00014-84-K-0564 from the Office of Naval Research.

2 Enumeration of Primitive Contacts

We assume that a high-level assembly planner (Liu 1990; Popplestone, Ambler & Bellos 1980) has supplied a nominal trajectory, a sequence of connected line segments in $\Re^6$ describing the motion of a *moving part* relative to a *stationary part*. We are also provided with geometric models of the parts, along with a set of *critical points*, i.e., poses at which the set of contacting surface features change (see figure 1a). The contacts that can arise in the presence of insertion clearances are determined by examining the contacts occurring at the critical points prior to introducing clearances to the models (see figure 1b). Any contact between the surface features of two polyhedral objects can be represented as a combination of *primitive contacts*: vertex-face, face-vertex, or edge-edge pairs (where each pair denotes moving and stationary part features, resp.) involving convex vertices and edges. The n primitive contacts $P_1, \ldots, P_n$ associated with a critical point are enumerated by detecting coincident features in the clearance-free models. The vertex-face contacts consist of all pairs (V, F) where convex vertex V lies within the polygon of face F. Face-vertex contacts are similar. Edge-edge contacts involve pairs (E_1, E_2) of convex edges whose line segments intersect.

Small clearances are now added to the models at the insertion sites by "shrinking" various dimensions of the moving part, stationary part, or both. In figure 2a, for example, clearances are introduced by receding a hole wall along its negated normal by a distance dc. Model dimension errors are represented by the displacment $\mathbf{dr} = [dr_x dr_y dr_z]^T$ of V from its model to actual position, and scalar dr_w, the displacement of F along its normal. These model error variables are subject to tolerances $|dr_i| \leq \epsilon_i,\ i \in w, x, y, z$.

3 Linearized C-Surfaces

Each primitive contact P_i that can occur around a critical point in the trajectory is characterized by a *linearized C-surface* in $\Re^{t+6}$, consisting of the tangent hyperplane to the actual C-surface of moving part poses associated with P_i. Following (Donald 1986), we represent model error variables as additional *dofs* in a generalized C-space. Linearized C-surfaces for vertex-plane and edge-edge contacts subject to model error are derived as follows.

Figure 2a shows a vertex V of the moving part and a face F of the stationary part, separated by a clearance dc. Model error variables $\mathbf{dr}$ and dr_w displace V and F to their real positions. A perturbation of the moving part from the critical point is denoted by a twist $\mathbf{dX} = [\mathbf{dx}^T\ \ \delta\mathbf{x}^T]^T$ with differential translation and rotation vectors $\mathbf{dx}$, $\delta\mathbf{x}$ (resp.). The placement of V against F is expressed by stating that V and F have

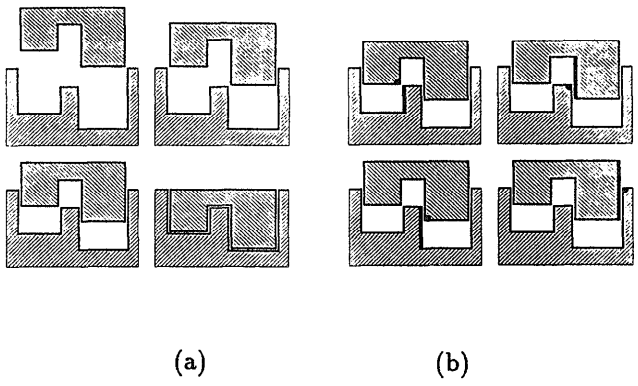

(a) (b)

Figure 1: (a) Critical points in a nominal trajectory. (b) Primitive contacts at a critical point.

the same ordinate along F's normal $\mathbf{n}$:

$$(\mathbf{p}+\mathbf{r}+\mathbf{dr}+\mathbf{dx}+\delta\mathbf{x}\times(\mathbf{r}+\mathbf{dr}))\cdot\mathbf{n} = (\mathbf{p}+\mathbf{r}-(dc+dr_w)\mathbf{n})\cdot\mathbf{n} \quad (1)$$

where $\mathbf{r}$ is the vector of displacement from the moving part's origin $\mathbf{p}$ to V. After eliminating the nonlinear term $(\delta\mathbf{x}\times\mathbf{dr})\cdot\mathbf{n}$, equation (1) may be expressed:

$$\begin{bmatrix} \mathbf{n} \\ \mathbf{r}\times\mathbf{n} \\ 1 \\ \mathbf{n} \end{bmatrix} \cdot \begin{bmatrix} \mathbf{dx} \\ \delta\mathbf{x} \\ dr_w \\ \mathbf{dr} \end{bmatrix} = -dc \quad (2)$$

which describes a hyperplane in $\Re^{10}$, whose normal is the left hand vector.

In figure 2b, edges E_1 and E_2 are subject to model error displacements $\mathbf{dr}_1$ and $\mathbf{dr}_2$ (resp.), and the edges are parallel to $\mathbf{v}_1$ and $\mathbf{v}_2$. Equating the ordinates of E_1 and E_2 along their mutual perpendicular $\mathbf{v}_1\times\mathbf{v}_2$ and dropping nonlinear terms yields:

$$\begin{bmatrix} \mathbf{v}_1\times\mathbf{v}_2 \\ \mathbf{r}_1\times(\mathbf{v}_1\times\mathbf{v}_2) \\ \mathbf{v}_1\times\mathbf{v}_2 \\ -\mathbf{v}_1\times\mathbf{v}_2 \end{bmatrix} \cdot \begin{bmatrix} \mathbf{dx} \\ \delta\mathbf{x} \\ \mathbf{dr}_1 \\ \mathbf{dr}_2 \end{bmatrix} = \mathbf{v}_1\times\mathbf{v}_2\cdot\mathbf{dc} \quad (3)$$

where $\mathbf{r}_1$ is the displacement from the moving part's origin $\mathbf{p}$ to point $\mathbf{q}_1$ on E_1, and $\mathbf{q}_1$ coincides with point $\mathbf{q}_2$ on E_2 prior to introducing clearance vector $\mathbf{dc}$. Equation (3) describes a hyperplane in $\Re^{12}$, whose normal consists of the lefthand vector. In general, linearized C-surfaces are constructed in a $(t+6)$-dimensional C-space, where t is the number of model dimensions subject to size tolerance.

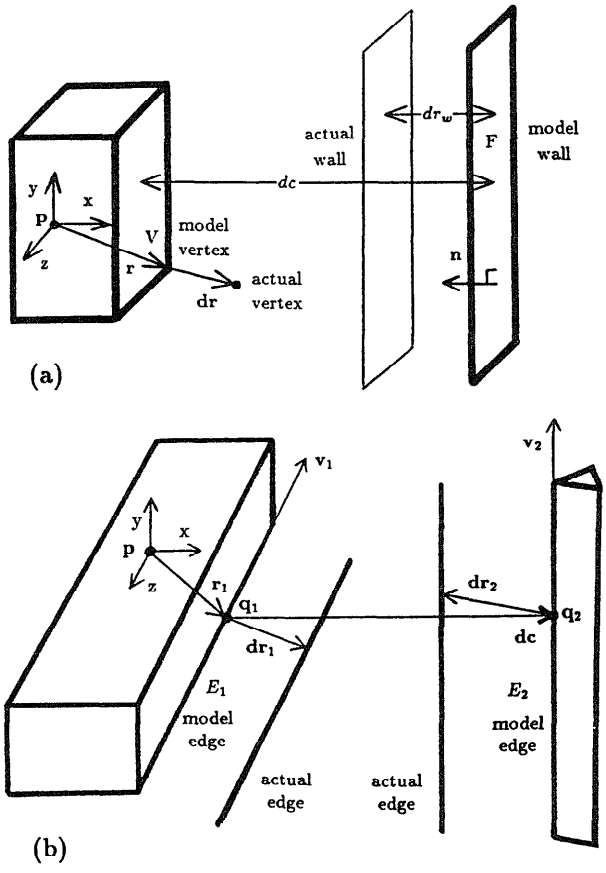

Figure 2: (a) A vertex-face contact. (b) An edge-edge contact.

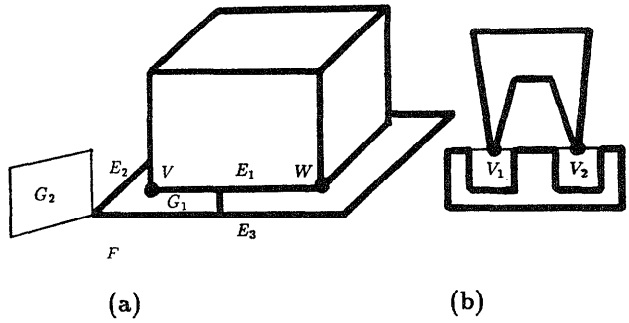

Figure 3: (a) A critical point in the nominal trajectory. (b) Rim vertices.

4 Convex Regions in C-Space

In addition to a linearized C-surface equation, our representation of a primitive contact's linearized C-surface must also include an inequality for each C-surface boundary arising from a real surface boundary. In figure 3a, the moving part is situated at the critical point at which its base is aligned with the outside rim face F of a hole in the stationary part. An edge E_1 of the moving part's base may contact one of the rim edges E_2, so we characterize this contact by a linearized C-surface, represented by the hyperplanar equality formulated in equation (3). For E_1 to contact E_2, however, E_1's vertex V must lie on the left side of hole wall G_1. This constraint may be represented by an inequality, bounded by equation (2). We thus establish a vertex-face C-surface as a barrier beyond which the edge-edge C-surface does not extend. Erecting a similar inequality constraint to represent the finite extent of E_2, the primitive contact between E_1 and E_2 is represented by a constraint set containing the original equality, plus two inequalities, in $\Re^{t+6}$.

In general, a primitive contact P_i is characterized as a convex, hyperplanar polytope H_i in $\Re^{t+6}$. Each polytope H_i is represented by a *constraint set* S_i consisting of a single equation and a number of inequalities in $\Re^{t+6}$, as one might represent a polygon in $\Re^2$. Primitive contact constraint sets may also include artificial constraints involving imaginary faces, such as G_2 in figure 3a, which splits the concave primitive contact between V and F into two convex primitive contacts.

The set of nonoverlapping configurations surrounding a critical point, denoted by set "*LEGAL*", is also concave but can be constructed as a union of convex volumes $\mathcal{L}_1, \ldots \mathcal{L}_m$ in $\Re^{t+6}$. The planar moving part in figure 3b, for example, moves in a 3−dimensional C-space whose subset *LEGAL* is concave, owing to the convex hole rims. This C-space may be partitioned into four convex volumes in $\Re^3$, corresponding to the four possible assignments of the two vertices to the convex regions above or below their adjacent hole rims. Each volume $\mathcal{L}_i$ may be represented by artificial constraints confining each of V_1 and V_2 to its assigned convex region, plus constraints prohibiting overlap between a vertex and a hole wall. Assuming all concavities in *LEGAL* arise from convex hole rims of the stationary part, we can generally characterize *LEGAL* as a union of convex volumes $\mathcal{L}_i$, where each $\mathcal{L}_i$ corresponds to an assignment of the moving part's "rim vertices" to halfspaces on one side or the other of their adjacent stationary part hole rims. (Dakin 1991) describes the construction of sets $\mathcal{L}_i$ for 3-dimensional assembly parts.

5 Generating Paths in Contact Space

Once the primitive contacts $P_1, \ldots, P_n$ that may occur around a critical point are characterized by their hyperplanar polytopes $H_1, \ldots, H_n$ and corresponding constraints sets $S_1, \ldots, S_n$, we can determine through linear programming which combinations of primitive contacts might occur simultaneously. A *contact state* $C = \{P'_1, \ldots, P'_k\}$ is a k-element subset of $\{P_1, \ldots, P_n\}$, such that $P'_1, \ldots, P'_k$ can coexist in C-space without overlap, and without necessarily the presence of an additional P'_l. The contact states $C_1, \ldots, C_m$, plus the empty set $\emptyset$ and $\{P_1, \ldots, P_n\}$, form a lattice under the relation of set inclusion (Koutsou 1986). The region in C-space represented by a contact $C = \{P'_1, \ldots, P'_k\}$ is the intersection $(\bigcap_{i=1}^{k} H'_i) \cap LEGAL$ of the primitive contacts' polytopes with $LEGAL$. We shall refer to a contact state C as an *n-dimensional state* if its tangent space in $\Re^{t+6}$ has rank n, or equivalently, if the vector space spanned by the H'_is' hyperplanar normals has rank $t + 6 - n$.

To generate tentative paths of traversal in the contact space around a critical point, we require computational tools to (1) decide if a set of primitive contacts forms a contact state, and (2) identify its adjacent states. As for (1), k primitive contacts $P'_1, \ldots, P'_k$ can coexist without overlap iff $(\bigcap_{i=1}^{k} H'_i) \cap \mathcal{L}_j \neq \emptyset$ for some convex component $\mathcal{L}_j$ of $LEGAL$. This decision is performed as a linear programming feasibility test involving constraint sets $S'_1, \ldots S'_k$ of the k primitive contacts and the constraint set $\mathcal{S}_j$ of $\mathcal{L}_j$. We moreover determine whether $\{P'_1, \ldots, P'_k\}$ can coexist without any additional contact P'_l by determining if $\{P'_1, \ldots, P'_k, \bar{P}'_l\}$ can coexist without overlap, where imaginary contact $\bar{P}'_l$ represents a slightly separated P'_l contact. Regarding (2), we enumerate the contact states C' adjacent to a given state $C = \{P'_1, \ldots, P'_k\}$ by adding or subtracting a P'_i and checking that the new combination is a valid contact state.

The decision procedures described above may be utilized to generate candidate sequences of traversable contact states around each successive critical point. As seen in the contact state graph in figure 4a, for example, the assembly motion begins in free space $C_0 = \emptyset$. The 1-point contact states surrounding the first critical point include an edge-edge contact state C_1 and a vertex-plane contact state C'_1. After verifying the legality of these states, we choose (say) C_1 and enumerate its adjacent 2−point contact states, which include C_2 and C'_2, and so on. The final contact state in the selected sequence must be shared by the contact state lattice associated with the next critical point, where it will serve as the initial contact state in the next sequence of contact states.

6 Command Velocity Synthesis

Once a path of contact states $C_0, \ldots, C_m$ is selected for traversing the contact space around a critical point in the nominal trajectory, we specify *target poses* in some or all of the contact states. Each target pose $\mathbf{dX}_i \in \Re^6$ is a perturbation of the assembly's pose away from the critical point. In the case of the first critical point, the initial target pose $\mathbf{dX}_0$ serves as the approach position in free space to which the moving part is (say) visually servoed. Every $\mathbf{dX}_i$ thereafter is the goal point associated with a contact state transition involving the establishment of an additional primitive contact, i.e., a transition to a lower-dimensional contact state (see figure 5a). The target poses $\mathbf{dX}_0, \ldots, \mathbf{dX}_l$ associated with a contact state sequence $C_0, \ldots, C_m$ (with $l \leq m$) comprise a *perturbed nominal trajectory* (PNT) in the contact state lattice surrounding the critical point.

A human designer may specify the target pose in a contact state by constraining any *dofs* in the assembly configuration left unconstrained by the primitive contacts. In figure 4b, the target pose in a contact state involving a single edge-edge contact is specified by supplying five "virtual" vertex-face contacts involving imaginary faces formed by perturbing existing faces by various distances d_i. Constraining the pose of an assembly to a single point $\mathbf{dX}_i$ in $\Re^6$ generally requires $6 - k$ such artificial constraints, where k is the rank of the space spanned by the primitive contacts' normals. As shown in figure 5a, each adjacent pair of target poses $\mathbf{dX}_i, \mathbf{dX}_{i+1}$ gives rise to a unit command velocity $\mathbf{v}_i$ parallel to $\mathbf{dX}_{i+1} - \mathbf{dX}_i$. When the fine-motion plan executes, recognition of each new contact via force sensing triggers the next command velocity.

After selecting a PNT within the chosen sequence of contact states, we must ensure that trajectory deviations arising from position and control error will not give rise to undesired contact state transitions. At the start of the assembly operation, the pose of the moving part is confined to an uncertainty region R_0 in $(t + 6)$-dimensional free space. As shown in figure 5a, we "verify" a candidate PNT by recursively forward-projecting the current uncertainty region R_i in contact state S_i, to obtain the uncertainty region R_{i+1} in the next contact state S_{i+1} that contains a target pose. Each R_i sweeps out a forward-projection volume F_i centered around command velocity $\mathbf{v}_i$ and (due to velocity uncertainty) expanding laterally to $\mathbf{v}_i$.

We employ a linear-programming feasibility test to determine if a forward-projection F_i intersects any undesired primitive contact's polytope H_j. A positive test result shows that for *some* universe allowed by the part dimension tolerances, an undesired contact state transition *might* occur, due to position and con-

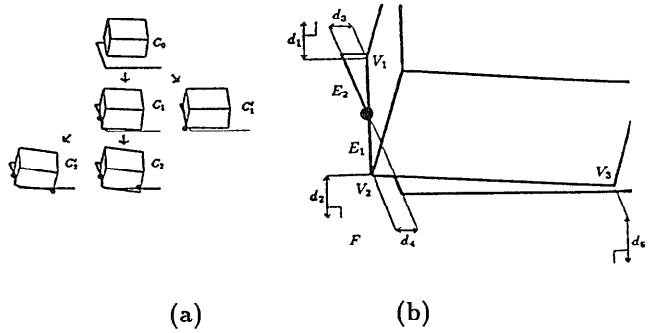

Figure 4: (a) Alternative sequences of contact states. (b) Specifying a target pose in a contact state.

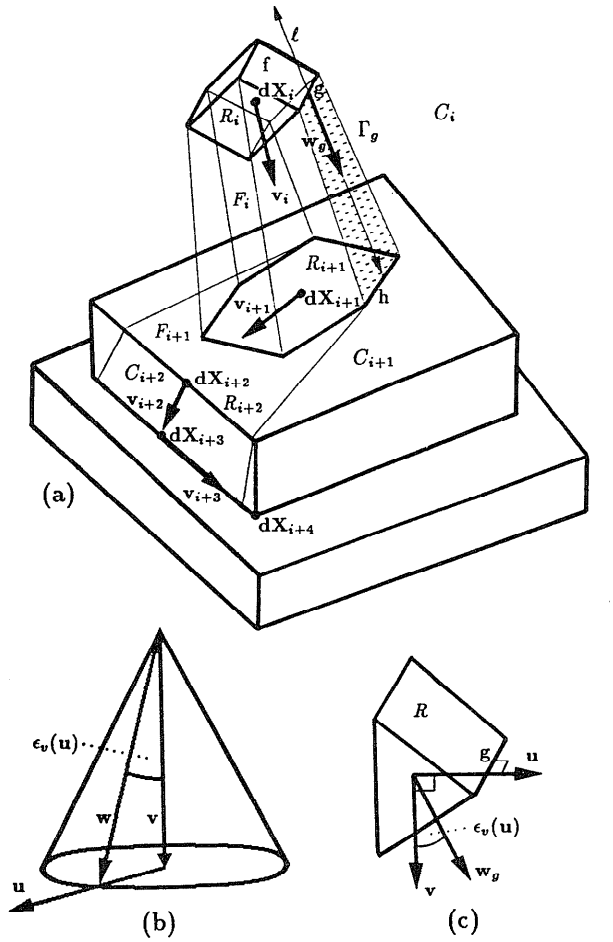

Figure 5: (a) Uncertainty analysis in C-space. (b) Control velocity error cone. (c) Deriving the motion of an uncertainty region facet.

trol error. Accordingly, the PNT, the clearances, or the tolerances must be modified. Tightening the tolerances permits the forward-projections to bypass the unwanted contacts more easily. But since tighter tolerances increase the cost of manufacturing the parts (Fortini 1967), it is desirable to obtain a fine motion strategy with as wide tolerance ranges as possible. If F_i is shown not to intersect any undesired primitive contacts' polytopes in $\Re^{t+6}$, then the command velocity $\mathbf{v}_i$ defined by the sequential target poses $\mathbf{dX}_i$ and $\mathbf{dX}_{i+1}$ is valid. To verify subsequent command velocities, the process repeats by forward-projecting the uncertainty region R_{i+1} from S_{i+1} to S_{i+2}, and so on.

As seen in figure 5a, the forward-projection F_i of a 3−dimensional region R_i is bounded by planes, such as Γ_g, formed by translating a 1−dimensional facet g along some deviating velocity $\mathbf{w}_g$. A 1−dimensional facet g gives rise to such a bounding plane of F_i iff g does not pierce the interior of R_i when displaced along $\pm\mathbf{w}_g$. Only 6 of the 12 1−dimensional facets so qualify. We assume that the maximum angular deviation of a control velocity $\mathbf{w}$ from the command velocity $\mathbf{v}$ is available as a function $\epsilon(\mathbf{u})$ of the lateral deviation direction $\mathbf{u} \perp \mathbf{v}$ (see figure 5b). When calculating g's deviating velocity $\mathbf{w}_g$, we choose $\mathbf{u} \perp \mathbf{v}, g$, as shown in figure 5c. The resulting constraint plane Γ_g defines a halfspace which contains all possible trajectories from g. Γ_g and five similarly derived constraint planes define the boundary of F_i, together with constraint planes associated with C_{i+1} and the 3 "upper" 2−dimensional facets of R_i in figure 5a. A more general algorithm for forward-projecting an n-dimensional uncertainty region is described in (Dakin 1991).

7 Discussion

Our methodology for designing a fine motion strategy permits the designer to select clearances and tolerances that will facilitate the search for a verifiable sequence of command velocities. This approach is consistent with the view that a product should be designed with the feasibility of its assembly in mind (Whitney, et al. 1989). Other important criteria for selecting tolerances include machining costs, product function and performance, and stability during assembly.

We have highlighted the earliest stages in a mating operation, in which the moving part traverses the contact state lattice around the first critical point encountered in the trajectory. Traversal of this lattice begins in a region R_0 surrounding the initial target pose in free space. If there is more than one critical point, then the goal state in the first lattice must be present in the second lattice, where it serves as the initial state in the second sequence. The traversal of a contact state shared by two lattices constitues a *global* transit

between two critical points. To restrict the pose uncertainty resulting from such a transit, we must force the assembly to follow multiple-contact states, i.e., the crevices and corners of C-space (Koutsou 1986).

The designer tools described in sections 2 – 6 have been implemented in the POPLOG environment running on a Sun 3 workstation. Surface descriptions of CSG-modelled assembly parts are obtained from a geometric modeller (Brown 1982) and placed in POP-11 records, which serve as nodes in an adjacency graph of part facets (Dakin, et. al 1989). Geometric data from the models parameterize linearized C-surface equations (2) and (3), to generate the contraint sets representing the primitive contacts' hyperplanar polytopes, as well as the convex components of *LEGAL*. A FORTRAN simplex procedure is employed to perform the feasibility tests mentioned in sections 5 and 6. Wrench constraints for jamming avoidance and contact maintenance in the chosen contact states are also generated (Dakin 1991). Fine motion strategies for traversing contact state sequences, similar to those in figure 4a, have been designed interactively with this system.

With a view toward further automation, future research will explore the heuristic generation of command velocities (Laugier 1989) and contact state sequences. We also seek to extend the domain of our approach to assembly parts with quadric surfaces.

8 Conclusion

A methodology for augmenting a nominal assembly motion plan with a fine-motion strategy was introduced. Linearizations of C-space around critical points in the trajectory enabled us to use linear programming to synthesize *perturbed nominal trajectories* for traversing local, polytopic contact spaces in the presence of position, control, and model error.

References

Brown, C.M. 1982. PADL2: A Technical Summary. *IEEE Computer Graphics Applications* 2(2):69-84.

Brooks, R.A. 1982. Symbolic Error Analysis and Robot Planning. *Int. Journal of Robotics Res.* 1(4):29-68.

Caine, M.E. 1985. Chamferless Assembly of Rectangular Parts in Two and Three Dimensions. Masters Thesis, Dept. of Mechanical Engineering, MIT.

Dakin, G. 1991. Augmenting a Nominal Assembly Motion Plan with a Compliant Behavior. Tech. Report 91-6, Dept. of COINS, Univ. of Mass., Amherst Mass.

Dakin, G., Liu, Y., Nair, S., Popplestone, R.J., Weiss, R. 1989. Symmetry inference in planning assembly. In Proceedings of the IEEE International Conference on Robotics and Automation. 1865-1868. Scottsdale, AR, May 1989.

Donald, B.R. 1986. Robot Motion Planning with Uncertainty in the Geometric Models of the Robot and Environment: A Formal Framework For Error Detection and Recovery. In Proceedings of the IEEE International Conference on Robotics and Automation. 1588-1593. San Francisco, CA. 1986

Fortini, E.T. 1967. *Dimensioning for Interchangeable Manufacture.* New York: Industrial Press.

Koutsou, A. 1986. Parts Mating by Moving Objects in Contact. PhD Thesis, Dept. of Artificial Intelligence, Edinburgh University.

Latombe, J.C. 1989. Motion Planning with Uncertainty: on the Preimage Backchaining Approach. In Khatib, O., Craig, J., Lozano-Pérez, T. eds. *The Robotics Review.* Cambridge, Mass.: MIT Press.

Laugier, C. 1989. Planning Fine Motion Strategies by Reasoning in Contact Space. In Proceedings of the IEEE International Conference on Robotics and Automation. 653-659. Scottsdale, AR, May 1989.

Liu, Y. 1990. Symmetry Groups in Robotic Assembly Planning. PhD Diss., Dept. of COINS, Univ. of Mass., Amherst, Mass.

Lozano-Pérez, T., Mason, M., Taylor, R.H. 1984. Automatic Synthesis of Fine-Motion Strategies for Robots. *International Journal of Robotics Research* 3(1):3-24.

Popplestone, Ambler, A.P., Bellos, I. 1980. An Interpreter for a Language Describing Assemblies. Artificial Intelligence 14(1):79-107.

Taylor, R.H. 1976. A Synthesis of Manipulator Control Programs from Task-Level Specifications. Memo AIM-282, A.I. Lab, Standford Univ.

Whitney, D.E. 1982. Quasi-Static Assembly of Compliantly Supported Rigid Parts. *Journal of Dynamic Systems, Measurement, and Control* 104:64-77.

Whitney, D.E., De Fazio, T.L., Gustavson, R.E, Graves, S.C., Abell, T., Cooprider, C., Pappu, S. 1989. Tools for Strategic Product Design. In Proceedings of the NSF Engineering Design Research Conference. 581-595. Univ. of Mass., Amherst, Mass. 1989.